Molecular modeling study toward development of H_2S-free removal of iron sulfide scale from oil and gas wells

Buijs, Wim; Hussein, Ibnelwaleed A.; Mahmoud, Mohamed; Onawole, Abdulmujeeb T.; Saad, Mohammed A.; Berdiyorov, Golibjon R.

DOI
10.1021/acs.iecr.8b01928

Publication date
2018

Document Version
Final published version

Published in
Industrial and Engineering Chemistry Research

Citation (APA)
Buijs, W., Hussein, I. A., Mahmoud, M., Onawole, A. T., Saad, M. A., & Berdiyorov, G. R. (2018). Molecular modeling study toward development of H_2S-free removal of iron sulfide scale from oil and gas wells. *Industrial and Engineering Chemistry Research*, *57*(31), 10095-10104. https://doi.org/10.1021/acs.iecr.8b01928

I&EC research
Industrial & Engineering Chemistry Research

Article

Cite This: Ind. Eng. Chem. Res. 2018, 57, 10095−10104

pubs.acs.org/IECR

Molecular Modeling Study toward Development of H_2S-Free Removal of Iron Sulfide Scale from Oil and Gas Wells

Wim Buijs,*[,†] Ibnelwaleed A. Hussein,[‡] Mohamed Mahmoud,[§] Abdulmujeeb T. Onawole,[‡] Mohammed A. Saad,[∥] and Golibjon R. Berdiyorov[⊥]

[†]Engineering Thermodynamics, Process & Energy Department, Delft University of Technology, Leeghwaterstraat 39, 2628 CB Delft, The Netherlands

[‡]Gas Processing Center, College of Engineering, Qatar University, P.O. Box 2713, Doha, Qatar

[§]Department of Petroleum Engineering, King Fahd University of Petroleum & Minerals, Dhahran 31261, Saudi Arabia

[∥]Chemical Engineering Department, College of Engineering, Qatar University, P.O. Box 2713, Doha, Qatar

[⊥]Qatar Environment and Energy Research Institute, Hamad Bin Khalifa University, P.O. Box 5825, Doha, Qatar

Supporting Information

ABSTRACT: A common problem that faces the oil and gas industry is the formation of iron sulfide scale in various stages of production. Recently an effective chemical formulation was proposed to remove all types of iron sulfide scales (including pyrite), consisting of a chelating agent diethylenetriaminepentaacetic acid (DTPA) at high pH using potassium carbonate (K_2CO_3). The aim of this molecular modeling study is to develop insight into the thermodynamics and kinetics of the chemical reactions during scale removal. A cluster approach was chosen to mimic the overall system. Standard density functional theory (B3LYP/6-31G*) was used for all calculations. Low spin $K_4Fe(II)_4(S_2H)_{12}$ and $K_3Fe(II)(S_2H)_5$ clusters were derived from the crystal structure of pyrite and used as mimics for surface scale FeS_2. In addition, K_5DTPA was used as a starting material too. High spin $K_3Fe(II)$DTPA, and K_2S_2 were considered as products. A series of $K_mFe(II)(S_2H)_n$ complexes ($m = n-2$, $n = 5-0$) with various carboxylate and glycinate ligands was used to establish the most plausible reaction pathway. Some ligand exchange reactions were investigated on even simpler Fe(II) complexes in various spin states. It was found that the dissolution of iron sulfide scale with DTPA under basic conditions is thermodynamically favored and not limited by ligand exchange kinetics as the activation barriers for these reactions are very low. Singlet−quintet spin crossover and aqueous solvation of the products almost equally contribute to the overall reaction energy. Furthermore, seven-coordination to Fe(II) was observed in both high spin $K_3Fe(II)$DTPA and $K_2Fe(II)(EDTA)(H_2O)$ albeit in a slightly different manner.

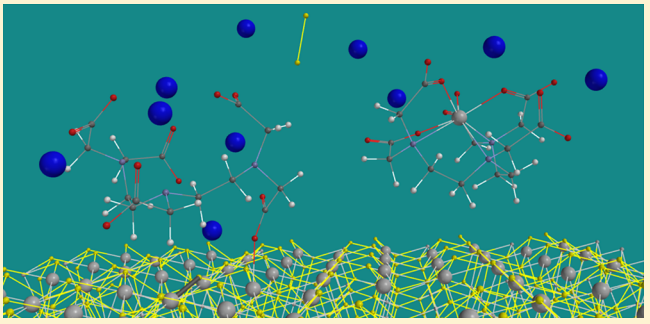

INTRODUCTION

One of the common problems in oil and gas industry is the formation of an iron sulfide scale, which has an adverse impact on the performance of both subsurface (casings, production tubing, mandrels, and pipelines) and surface (pumps, heating turbines, and heat exchangers) production equipment.[1−4] Depending on external conditions and reactant environment,[5] iron sulfides exist in several distinct crystalline forms with different ratios of iron to sulfur and, consequently, with different physical and chemical properties, including troilite (FeS), marcasite (FeS_2), pyrite (FeS_2), and pyrrhotite (Fe_7S_8).[6] Scale deposition depends on different factors such as temperature, pH, pressure, chemical reactions and equilibria, contact time, evaporation, and ionic strength.[5] Deposition of scale can occur as a single mineral phase. However, a combination of different phases is often observed. The most common types of scales encountered during oil and gas production include sulfates which are formed by mostly group II metals such as barium, strontium, and calcium; oxides/hydroxides which are formed by iron and magnesium; carbonates which are formed by calcium; and sulfides which is formed by iron.[7,8]

It is estimated that the total annual cost of corrosion (which occurs due to scaling) in the oil and gas production industry is 1.372 billion US$. About $589 million US$ is due to surface pipeline and facility costs, while 463 million US$ goes to downhole tubing costs and another 320 million US$ in capital expenditures.[9−11] A case study on the effect of scale deposition was carried out between 1995 and 1997 in the production system of Tinggi oilfield in offshore Terengganu, Malaysia.

Received: May 4, 2018
Revised: June 24, 2018
Accepted: July 5, 2018
Published: July 5, 2018

This field experienced a sharp production decline within those 2 years at a rate of 26% per year.[12]

A common practice in petrochemical industry in removing iron sulfide scales involves usage of hydrochloric acid (HCl) and other mineral acids.[13] However, the efficiency of such conventional methods strongly depends on the composition and the crystalline structure of the scale. For example, HCl results in better dissolution when the molar ratio of iron to sulfide is close to unity, whereas iron disulfide has very low solubility in HCl.[14] Another important issue arising from the chemical treatment of iron sulfide scales is the formation of toxic gases such as H_2S [13] which cause serious health and environmental problems. Other chemical solutions include the use of organic acids and chelating agents. The former has the demerit of being costly and of showing a rather poor record in performance as compared to HCl in dissolving carbonate scales. However, chelating agents such as EDTA, DTPA, HEDTA, and GLDA seem to be a better alternative than HCl. Aside from chemical removal of scale, drilling, as a mechanical way, is applied as a last resort despite being complicated and increasing the corrosion rate by creating dips. Hence, a chemical treatment is preferred.[15]

Recently, Mahmoud et al.[16] proposed a new alternative chemical formulation to remove all types of iron sulfide scales, including the most common and thermodynamically very stable iron sulfide mineral pyrite.[17] It consists of DTPA and a converting agent (K_2CO_3) at a pH of 11−14. DTPA is promising because it is a polydentate ligand for Fe(II) using both COO^- and amine groups.[18] In addition, DTPA is less corrosive and has one of the highest stability constant among other chelating agents.[19] Depending on the concentration of DTPA and K_2CO_3, a maximum efficiency of 85% has been reached for pyrite, largely exceeding the 20% efficiency of scale removal with HCl, while no H_2S gas has been released. This makes the novel approach environmentally much more friendly and reduces the operational cost. Optimizing the system requires fundamental understanding of the actual chemical reactions and the role of the various components and process conditions (chelating agent, base, pH).[20,21]

Molecular modeling can be an attractive alternative to explore the large number of optimization possibilities. However, the system under consideration is very challenging because it involves the reaction of a solid surface of FeS_2 scale (pyrite) with a chelating agent (DTPA) in a basic (K_2CO_3) aqueous environment. There is no experimental information available on either the actual surface structure of pyrite scale or the wetting behavior under the actual process conditions. Therefore, a harsh simplification has been made to adopt a small cluster approach using standard DFT calculations to get a first impression of the thermodynamics and the kinetics of the dissolution of FeS_2 scale with DTPA in the presence of K_2CO_3.

COMPUTATIONAL DETAILS

All molecular simulations were performed using Wavefunction's Spartan'16 suite.[23] All structures were fully optimized using density functional theory (DFT) within the standard B3LYP/6-31-G* functional starting from experimentally known structures, MMFF or PM6 geometries. Spin states are listed in the file names with s = singlet (0 unpaired electrons) and q = quintet (4 unpaired electrons. It turned out that the total energy of the also possible triplets was between the singlet and the quintets, and they are further neither discussed nor mentioned. All high spin (quintet) equilibrium geometries have been checked for stability.[39] Transition states were identified and characterized using their unique imaginary vibrational frequency. The conductor-like polarizable continuum model (C-PCM)[22] was used in combination with standard DFT. As a result of the huge simplifications in the system, reaction energies and activation barriers were estimated from total energies only. Quantitative results of all calculations and all molecular (ensemble) structures are available in Supporting Information.

RESULTS

Fe(II) complexes generally show complex electronic behavior. Electronically, Fe(II) is a d^6-system and can be present as a singlet (0 unpaired electrons), triplet (2 unpaired electrons), and a quintet (4 unpaired electrons). Experimentally all of them can be observed, either as single species or in equilibrium, depending strongly on the number and type of coordination and process conditions. Computationally they offer two challenges:

(1) Determining the correct structure of the Fe(II) complexes with various spin states;
(2) Determining the correct energies between Fe(II) complexes with various spin states.

DFT calculations, including B3LYP, usually show a good track record in task 1, while task 2 remains a challenge. Several publications in this field are listed,[24−28] most of them from a computational perspective as real experimental data are scarce. The determination of the correct energies between Fe(II) complexes with various spin states depends on two factors: (1) the spin pairing energy and (2) the ligand field energy, which together make up the energy of the complex for a spin state.

(1) Spin Pairing Energy. The calculated energy difference which can be considered as the spin pairing energy between the Fe(II) ion as singlet and quintet is 384 kJ/mol in favor of the quintet, whereas 229 kJ/mol is reported in the literature.[38] B3LYP/6-31G* thus overestimates the spin pairing energy of the naked Fe(II) ion ∼70% by favoring the quintet state. There is general agreement in the literature cited above that this overestimate is related to the amount of HF exchange in hybrid DFT codes. B3LYP/6-31G* uses the original unmodified exchange of 0.2000 Hartree−Fock + 0.0800 Slater + 0.7200 B88. B3LYP* uses a lower amount of HF exchange. Most, if not all, hybrid functionals follow the same trend in varying the amount of HF exchange[24] to obtain better spin pairing energies. On the other hand, standard GGA functionals like PB86, PW91, PBE, and RPBE overestimate the singlet state. Furthermore, varying basis sets, for example, from 6-311+G* to the smaller 6-31G*, have a small but distinct effect on the energetics, but similar trends are observed.

(2) Ligand Field Energy. Ligands do affect the splitting of the energy level of the d-electrons.[33] Ligands with a low field (small energy difference between the singlet and the quintet state) lead to high spin complexes, and ligands causing a large energy difference yield low spin complexes. The spectrochemical series[33] below depicts the strength of the ligands in ascending order.

$$\begin{aligned}&\text{(weak) } I^- < Br^- < S^{2-} < SCN^- < Cl^- < NO_3^- < N_3^-\\ &< F^- < OH^- < C_2O_4^{2-} \approx H_2O < NCS^- < CH_3CN\\ &< py < NH_3 < en < bipy < phen < NO_2^- < PPh_3\\ &< CN^- \approx CO \text{ (strong)}\end{aligned}$$

DOI: 10.1021/acs.iecr.8b01928
Ind. Eng. Chem. Res. 2018, 57, 10095−10104

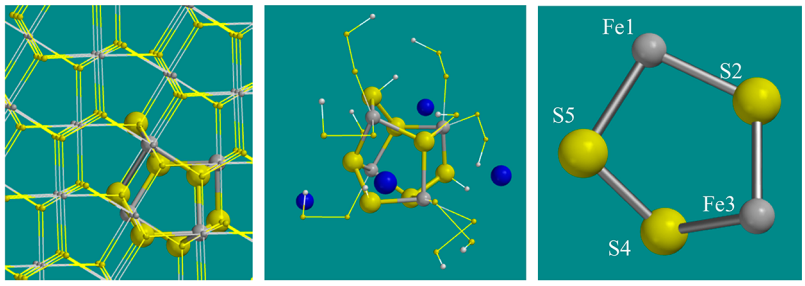

FeS_2 (pyrite lattice)[35] $K_4Fe(II)_4s(S_2H)_{12}$ 5-membered ring

Figure 1. Structures displayed as ball and wire. Pyrite lattice atoms used to construct the cluster, the actual cluster, and the typical five-membered ring are displayed as ball and spoke. K^+ ions in the cluster are displayed in blue, while Fe and S are gray and yellow, respectively.

DTPA as chelating agent shows tertiary amine and carboxylate ligands, while pyrite (FeS_2) has S_2^{2-} ligands only. The S_2^{2-} ligand is not in the list, but pyrite is experimentally known to be a low spin complex[34] by its absence of a magnetic moment. Furthermore, in a basic aqueous environment OH^- and H_2O can act as ligands. The OH^-, $C_2O_4^{2-}$, and H_2O ligands on octahedral Fe(II) will lead to high spin complexes.[33] The tertiary amines present in DTPA might lead to low spin complexes.

In some slightly older studies,[27,32] a benchmark was presented using three six-coordinated Fe(II) complexes, $Fe(II)(H_2O)_6$, $Fe(II)(NH_3)_6$, and $Fe(II)(bpy)_3$, to compare a variety of DFT codes against high level CASPT2 calculations as a reference. Experimental data on the actual energy differences between spin states are not available for these complexes but the observed spin states are known. CASPT2 yields for $Fe(II)(H_2O)_6$ 210 kJ/mol in favor of the quintet state, which is actually not far away from the above-mentioned 229 kJ/mol for the spin pairing energy. For $Fe(II)(NH_3)_6$, 109 kJ/mol in favor of the quintet state and for $Fe(II)(bpy)_3$, 47 kJ/mol in favor of the singlet state was found. B3LYP/6-31G* yields 149, 64, and 17 kJ/mol for these complexes respectively (see Supporting Information for structures and energies). From these data it can be concluded that both CASPT2 and B3LYP/6-31G* in all cases predict the correct spin state of these complexes. On comparing the energy differences of the two spin states of these complexes between the two computational methods, no general conclusion can be drawn on the performance of B3LYP with respect to over- or underestimating spin states energies. B3LYP/6-31G* using 0.2000 HF-exchange and a small basis set (6-31G*) does not behave significantly different from a B3LYP* approach with a higher or lower amount of HF-exchange or one with an extended basis set. A linear correlation between CASPT2 and B3LYP/6-31G* total energy results could be established that will be used as an indication for the energy differences. The relation is

$$\Delta E_{(HS-LS)}(CASPT2) = 1.546\,\Delta E_{(HS-LS)}(B3LYP/6\text{-}31G^*) + 10.1 \ \text{(kJ/mol)}$$

The correlation for the prediction of $\Delta E_{(HS-LS)}(CASPT2)$ from $\Delta E_{(HS-LS)}(B3LYP/6\text{-}31G^*)$ is only reasonable with R^2 = 0.9821 and a rmsd = 14.1 kJ/mol. The relation will be used as a part of the estimate on the overall thermodynamics of the dissolution of FeS_2 scale with DTPA under basic conditions. Next the results of several complexes mimicking the gradual transformation of pyrite scale by various ligand exchanges into Fe(II)DTPA will be discussed.

Figure 1 shows both the pyrite lattice and the cluster derived from it. In the pyrite lattice all Fe(II) ions are in octahedral coordination with six S_2^{2-} ligands and all S atoms are in tetrahedral binding mode with one covalent bond to the second S of the S_2^{2-} ligand and 3-fold coordination to Fe(II) ions, thus establishing the molar ratio in FeS_2. Another characteristic of the pyrite lattice is the presence of identical five-membered rings, puckered between Fe3−S4−S5, as displayed in Figure 1. Unique Fe−S distances in the ring are Fe1−S2 = 2.236 Å, S2−Fe3 = 2.259 Å, Fe3−S4 = 2.270 Å, S3−S5 = 2.155 Å, and S5−Fe1= 2.282 Å. The highlighted atoms in the lattice were taken out to create a pyrite type cluster with one free coordination site. This was done by terminating the additional S_2^{2-} ligands with H^+ and compensating the remaining negative charge with K^+ ions. K^+ was chosen as the chelating agent is K_5DTPA. Thus, the four Fe(II) ions in the cluster are all between slightly distorted square pyramidal and trigonal bipyramidal coordination to enable a possible "surface" reaction on the free coordination site. The K−S distances in the cluster range from 2.94 to 3.12 Å, depending on the specific environment. Fe−S distances in the cluster range from 2.22 ro 2.31 Å, the difference with the lattice being the result of the change from an S_2^{2-} ligand into an S_2H ligand, being in a cluster instead of a lattice, and the inherent error of DFT codes like B3LYP. It is important to stress the finding that the $K_4Fe(II)_4s(S_2H)_{12}$ cluster is stable in the singlet state only, in line with the experimental determination of the spin state of pyrite.[34]

Thus, an even simpler cluster was constructed to investigate the effect of the spin crossover on the structure $K_4Fe(II)(S_2H)_6$. Figure 2 shows $K_4Fe(II)(S_2H)_6$ in its singlet and quintet state. In order to allow an easy comparison of the two forms, the atomic labeling is displayed as well. Whereas the singlet is an octahedral complex with Fe−S distances ranging from 2.41 to 2.55 Å and with the 4 K^+ ions in almost tetrahedral arrangement evenly partitioned at the outside of the cluster, the quintet actually has decomposed into a $Fe(II)(S_2H)_5$ with square pyramidal coordination and a separate S_2H^- unit. The Fe−S distances in the quintet range from 2.48 to 2.59 Å for the coordinating S_2H ligands to 5.02 Å for the removed S_2H ligand. $K(2)^+$ and $K(3)^+$ keep the structure together and have moved to new positions. The difference in energy between the singlet and the quintet is 167 kJ/mol in favor of the quintet (B3LYP/6-31G*). It should be noted that a similar removal of a S_2H ligand in the singlet state is highly endothermic by 273 kJ/mol in the gas phase and 199 kJ/mol on aqueous solvation. So even a monomeric octahedral $K_4Fe(II)(S_2H)_6$ complex is stable as a singlet only. The next

DOI: 10.1021/acs.iecr.8b01928
Ind. Eng. Chem. Res. 2018, 57, 10095−10104

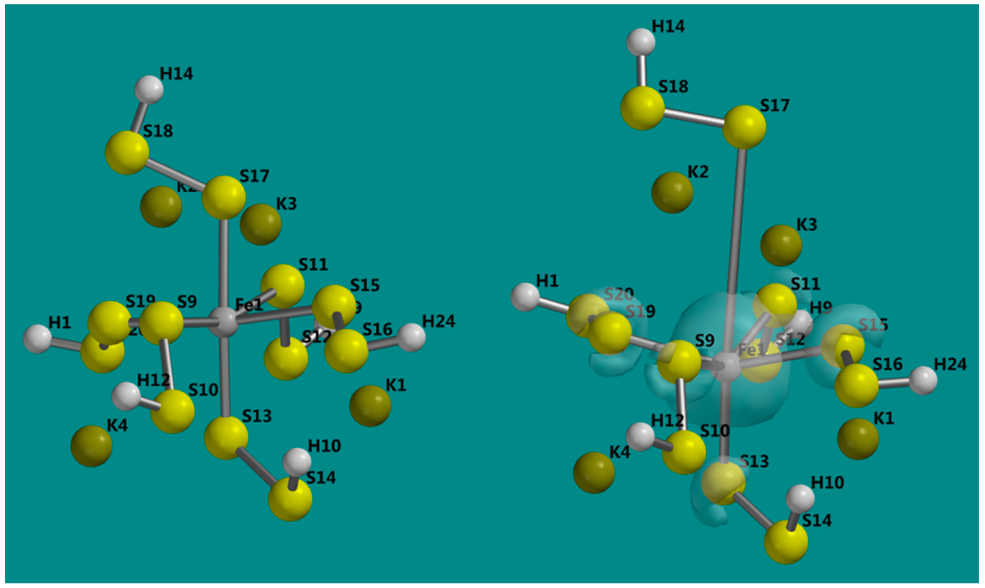

Figure 2. Structures displayed as ball and spoke with unique atomic numbering. The spin density on $K_4Fe(II)q(S_2H)_6$ is displayed too (B3LYP/6-31G*; surface: spin density (0.002 e/au^3)).

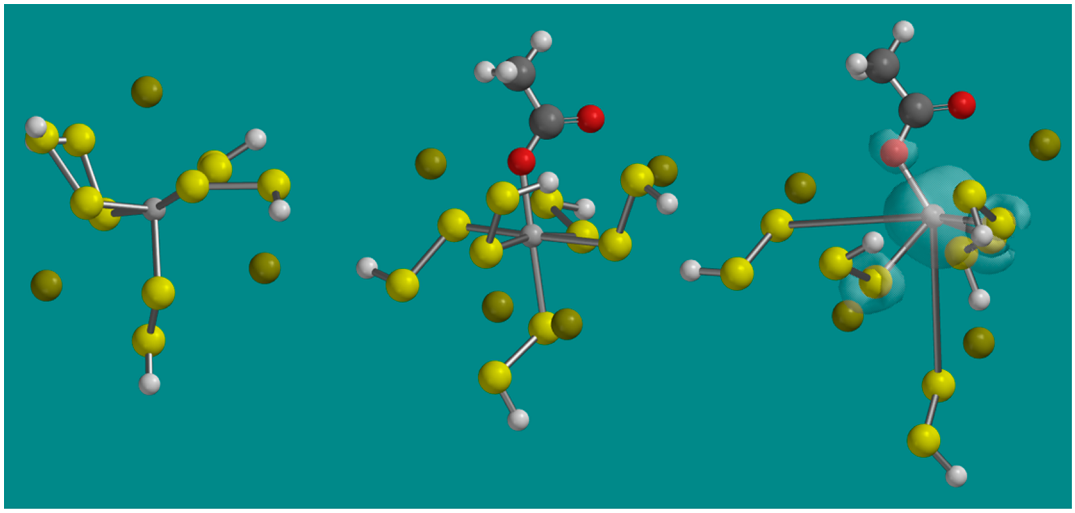

Figure 3. Structures displayed as ball and spoke; the spin density is displayed on the quintet too (B3LYP/6-31G*; surface: spin density (0.002 e/au^3)).

step was to investigate a monomeric Fe(II) cluster with five S_2H ligands.

Figure 3 shows $K_3Fe(II)s(S_2H)_5$, $K_4Fe(II)s(S_2H)_5(OAc)$, and $K_4Fe(II)q(S_2H)_5(OAc)$. It turned out that $K_3Fe(II)q(S_2H)_5$ is not stable and deteriorates to a tetrahedral Fe(II) complex with four S_2H ligands, loosely connected to the S_2H^- anion via two K^+ ions, very similar to $K_4Fe(II)q(S_2H)_6$. So this result strongly suggests that even a pyrite surface with Fe(II) ions in 5-fold coordination can exist only in the low spin state. The association of $K_3Fe(II)s(S_2H)_5$ with KOAc or KOAc (aq) to $K_4Fe(II)s(S_2H)_5(OAc)$ is −149 kJ/mol and −101 kJ/mol exothermic, respectively.

The spin crossover from $K_4Fe(II)s(S_2H)_5(OAc)$ to $K_4Fe(II)q(S_2H)_5(OAc)$ is −180 kJ/mol, i.e., an exothermic process. The structure has decomposed to a tetrahedral $K_2Fe(II)q(S_2H)_3(OAc)$ complex and two $K(S_2H)$ units, connected similarly via K^+-ions. The association of a carboxylate moiety with a five-coordinated $Fe(II)(S_2^{2-})_5$ species can be considered as the first step in the dissolution process of FeS_2 under the influence of K_5DTPA. The second step should be the spin crossover from singlet to quintet with the subsequent removal of two additional S_2^{2-} ligands. Both are exothermic processes. For the addition of KOAc (aq) to $K_3Fe(II)s(S_2H)_5$ yielding $K_4Fe(II)s(S_2H)_5(OAc)$ no activation barrier could be located. The activation barrier of the spin crossover reaction is unknown despite descriptions in previous literature[28,36] as a "radiationless nonadiabatic multiphonon process occurring between two distinct zero-order spin states characterized by different nuclear configurations", which means that there is virtually no activation barrier.

The association of an amine ligand of $K_3Fe(II)s(S_2H)_5$ with CH_3NH_2 to $K_3Fe(II)s(S_2H)_5(CH_3NH_2)$ was investigated too, as DTPA contains both amine and carboxylate ligands, and the descaling reaction might start from an amine as well. It turned

DOI: 10.1021/acs.iecr.8b01928
Ind. Eng. Chem. Res. 2018, 57, 10095−10104

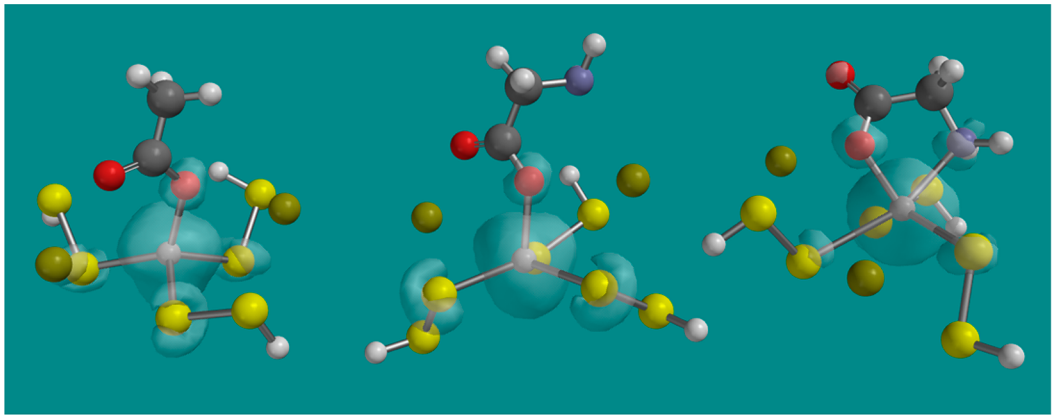

$K_2(Fe(II)q(S_2H)_3(OAc)$ $K_2(Fe(II)q(S_2H)_3(glycine\ md)$ $K_2(Fe(II)q(S_2H)_3(glycine\ bd)$

Figure 4. Structures displayed as ball and spoke. The spin densities are displayed too. Glycine md or bd is glycine monodentate or bidentate, respectively (B3LYP/6-31G*; surface: spin density (0.002 e/au^3)).

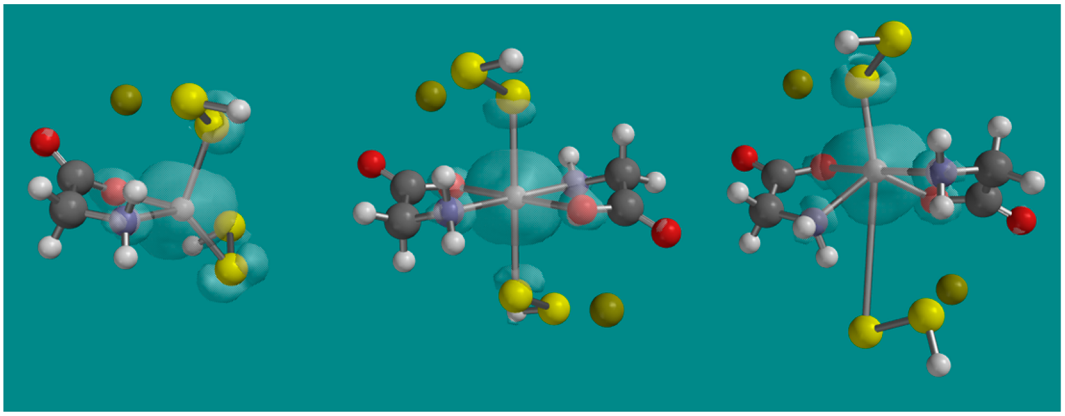

$KFe(II)q(S_2H)_2(gly\ bd)$ $K_2Fe(II)q(S_2H)_2(gly\ bd\ anti)_2$ $K_2Fe(II)q(S_2H)_2(gly\ bd\ syn)_2$

Figure 5. Structures displayed as ball and spoke. The spin densities are displayed too. Glycine md or bd is glycine monodentate or bidentate, respectively (B3LYP/6-31G*; surface: spin density (0.002 e/au^3)).

out that not only both the association reaction and the spin crossover are less exothermic (−79 and −136 kJ/mol, respectively), but much more importantly, no S_2H ligand is removed. So this reaction would result in a surface bound species only and not lead to the dissolution of the pyrite scale.

Thus, next the fate of the tetrahedral $K_2Fe(II)q(S_2H)_3(OAc)$ only will be investigated further. As the latter complex with three S_2H ligands still can be considered as a pyrite surface bound complex, additional ligand exchange reactions are needed to remove all S_2H ligands.

Figure 4 shows the approach: $K_2(Fe(II)q(S_2H)_3(OAc)$ was transformed into $K_2(Fe(II)q(S_2H)_3(glycine\ monodentate)$, and next into $K_2(Fe(II)q(S_2H)_3(glycine\ bidentate)$, as DTPA contains five glycidyl groups, capable of coordinating to Fe(II) by either its carboxylate group, its amino group, or both (bidentate). Fe−S distances range from 2.32 to 2.38 Å in $K_2(Fe(II)q(S_2H)_3(OAc)$ and $K_2(Fe(II)q(S_2H)_3(glycine\ md)$ to 2.37 Å in $K_2(Fe(II)q(S_2H)_3(glycine\ bd)$ for two S_2H ligands. One S_2H ligand is very loosely connected to Fe(II) with a distance of 2.87 Å; however still some residual spin density is present on the S.

Figure 5 shows the next step. The conversion of the $K_2(Fe(II)q(S_2H)_3(glycine\ monodentate)$ into $K(Fe(II)q(S_2H)_2(glycine\ bidentate)$ and $K(S_2H)$ seems to be an equilibrium reaction with a ΔE = −6.2 kJ/mol only. Again $K(Fe(II)q(S_2H)_2(glycine\ bidentate)$ is a tetrahedral complex.

If $K(Fe(II)q(S_2H)_2(glycine\ bidentate)$ associates with the second K^+-glycinate, two complexes can be the result: $K_2Fe(II)q(S_2H)(gly\ bd\ anti)_2$ with all ligands (O,N,S) opposite to each other (anti) and $K_2Fe(II)q(S_2H)(gly\ bd\ syn)_2$ with the O and N ligands on the same side (syn) but the S_2H ligands opposite. The highly symmetrical $K_2Fe(II)q(S_2H)(gly\ bd\ anti)_2$ shows a Fe−S distance of 2.62 Å, which is large compared to the Fe−S distance in $KFe(II)q(S_2H)_2(gly\ bd)$ of 2.29−2.39 Å. $K_2Fe(II)q(S_2H)(gly\ bd\ syn)_2$ shows two different Fe−S distances of 2.39 and 4.32 Å, respectively. Clearly the latter S_2H ligand has been removed from Fe(II) as it does not show any remaining spin density too. $K_2Fe(II)q(S_2H)(gly\ bd\ syn)_2$ is favored over $K_2Fe(II)q(S_2H)(gly\ bd\ anti)_2$ by −22.9 kJ/mol. $KFe(II)q(S_2H)(gly\ bd\ syn)_2$ is slightly distorted square pyramidal complex with an Fe−S distance of 2.48 Å. $KFe(II)q(S_2H)(gly\ bd\ syn)_2$ can associate with a third K^+-glycinate to yield $K_2Fe(II)q(gly\ bd\ syn)_3$. Figure 6 shows the result obtained.

Addition of glycinate by its amino group on the vacant coordination side in $KFe(II)q(S_2H)(gly\ bd\ syn)_2$ leads during geometry optimization initially to the octahedral $K_2Fe(II)q(S_2H)(gly\ bd\ syn)_2(gly\ md)$. However, $K_2Fe(II)q(S_2H)(gly\ bd\ syn)_2(gly\ md)$ is not an energy (local) minimum. An IR-frequency

DOI: 10.1021/acs.iecr.8b01928
Ind. Eng. Chem. Res. 2018, 57, 10095−10104

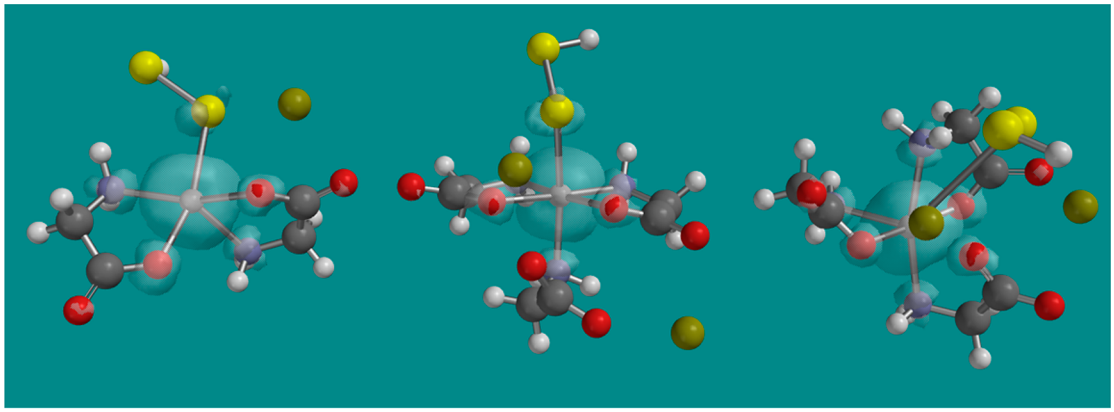

Figure 6. Structures displayed as ball and spoke. The spin densities are displayed too. Glycine md or bd is glycine monodentate or bidentate, respectively (B3LYP/6-31G*; surface: spin density (0.002 e/au^3)).

calculation yields four imaginary frequencies (ν = i78, i55, i31, and i17 cm^{-1}). The animations of two lower imaginary frequencies can be considered as a kind of reaction coordinate, and indeed the complex gradually transforms into $K_2Fe(II)q(S_2H)(gly\ bd)_3$ wherein the S_2H ligand is completely removed. Computational work on the structure of Fe-glycine complexes has been described before by Mandado et al.[37] They used B3LYP/6-311++G(d,p) and a similar solvation model. They concluded that bidentate ligand complexes are in all cases more stable than the corresponding monodentate ligand complexes. For B3LYP/6-31G* similar results were obtained. Thus, $KFe(II)q(gly\ bd)_3$ can be considered as the most stable entity in solution. Some care however is needed as their conclusions are based on solvent-entropy contributions to the overall ΔG's, as the ΔE-total (gas phase) favors $Fe(II)q(gly\ md)_3$ by 120 kJ/mol. In the present case the ΔE-total (gas phase) is 220 kJ/mol in favor of $K_2Fe(II)q(S_2H)(gly\ bd)_3$ instead of $K_2Fe(II)q(S_2H)(gly\ bd\ syn)_2(gly\ md)$. Mandado et al.[37] used charged complexes, and this work uses neutral complexes. This has a huge impact on any energy comparison, including solvation. Most likely this is the main reason for the difference observed. $KFe(II)q(gly\ bd)_3$ has some similarity with $K_3(Fe(II)(DTPA)$ and $K_2Fe(II)(EDTA)$ as all of them are multidentate Fe(II) complexes with amine and carboxylate ligands.

K_3Fe(II)DTPA and K_2Fe(II)(EDTA). DTPA is a complex multidentate ligand with ample modes of coordination to Fe(II) with three amine groups and five carboxylate groups. A conformer distribution (CD) of neutral $K_3Fe(II)DPTA$ complexes was obtained using molecular mechanics. A building scheme was used without a prebuild (octahedral) coordination mode to Fe(II) to avoid unrealistic outcomes. Thus, both Fe(II) and K^+ interactions with carboxylate anions were treated electrostatically only, as in an aqueous solution. No additional H_2O molecules were included at this stage.

From the possible 900 conformers, eventually 261 remained. Within the 261 conformers, there was still a considerable amount of redundancy present; particularly each carboxylate group produced two chemically identical conformers due to the molecular mechanics building scheme. A group of eight identical conformers show a relative strain energy of 0.00 kJ/mol and contribute to 86% in the cumulative Boltzmann weight. Actually, this group can be easily understood as it showed the perturbation of the C−O$^-$ and C═O of the four carboxylate groups, all coordinating with one oxygen to Fe(II) and another oxygen to one of two K^+ cations. The third K^+ cation coordinates to the $-N-(CH_2CO_2^-)$ group in the middle and one oxygen of a terminal $N-(CH_2CO_2^-)$ group. As the N atom in the middle is a point of symmetry which is recognized by the program, thus $2^4/2 = 2^3 = 8$ conformers yield. As all other conformers are at least 7 kJ/mol higher in energy, the conformational space of neutral $K_3Fe(II)DPTA$ complexes at normal temperatures seems quite limited. Figure 7 shows the major conformer of $K_3Fe(II)DPTA$ as obtained from the CD with MMFF and after geometry optimization with B3LYP/6-31G*. Like the complexes discussed above, the quintet state of Fe(II) is by far the most stable.

From Figure 7 it is clear that $K_3Fe(II)(DTPA)$ adopts a coordination with seven ligands in both MMFF and B3LYP/6-31G*. The spin density on Fe, the four carboxylate ligands, and the three amine ligands is instructive. The main difference between the MMFF and the B3LYP structure is the Fe−N distances with Fe−N1 = 2.998 Å, Fe−N2 = 3.485 Å, Fe−N3 = 2.484 Å and with Fe−N1 = 2.978 Å, Fe−N2 = 2.653 Å, Fe−N3 = 2.272 Å, respectively, and a slight change in position of one of the K^+ cations. The coordination of two N-ligands to Fe(II) is rather weak as the distances are 2.653 and 2.9778 Å. Fe−O (5,6,7) distances are slightly larger in the B3LYP quintet structure, which can be easily understood as MMFF was not parametrized for Fe(II) high spin structures.

Furthermore, the apparent preference of Fe(II) in the quintet state for O-ligands over N-ligands can be explained by the less directional character of the Fe−O interaction, compared to the Fe−N interaction, some additional strain in the DTPA-ligand, and last but not least, the required charge compensation the O-ligands offer to Fe(II).

An overview on seven-coordination in transition metal complexes was published in 2013.[30] Though seven-coordination is rather rare, polydentate ligands combined with a spherical electron distribution around the transition metal ion are obvious conditions stabilizing such a coordination mode. Among these complexes, $Na_2Fe(II)EDTA$ was already reported in 1993.[31] Figure 8, wherein the left part was taken from that publication, shows $Fe(II)(EDTA)(H_2O)$. The X-ray derived crystal structure Fe−OH_2 distance is 2.194 Å, the four Fe−O(carboxylate) distances are 2.174−2.198 Å, and the two Fe−N distances are 2.340 Å. It should be noted that the whole crystal structure is

DOI: 10.1021/acs.iecr.8b01928
Ind. Eng. Chem. Res. 2018, 57, 10095−10104

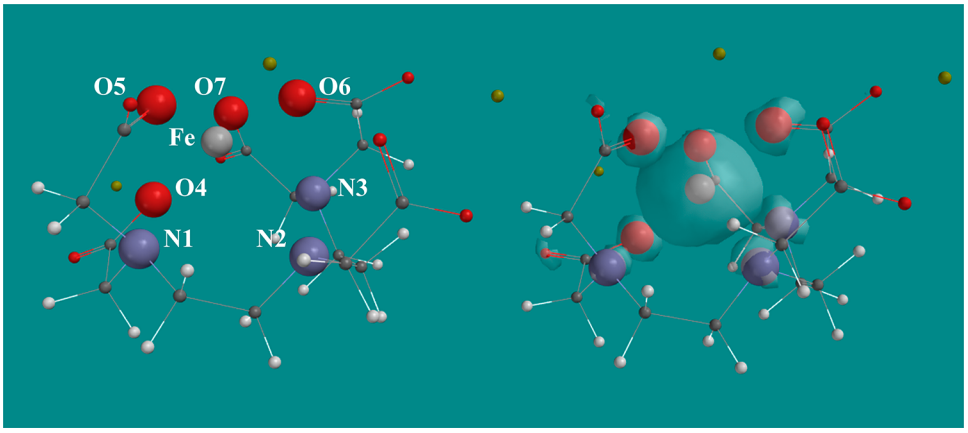

Figure 7. Major conformer of $K_3Fe(II)(DTPA)$ as derived from the CD with MMFF and after geometry optimization with B3LYP/6-31G* in the quintet spin state. Fe(II) and ligands coordinating to Fe(II) are displayed as ball and spoke and labeled in the MMFF structure, while all other atoms are displayed as ball and wire to reach maximum clarity. The B3LYP/6-31G* structure in addition shows the spin density (0.002 e/au^3).

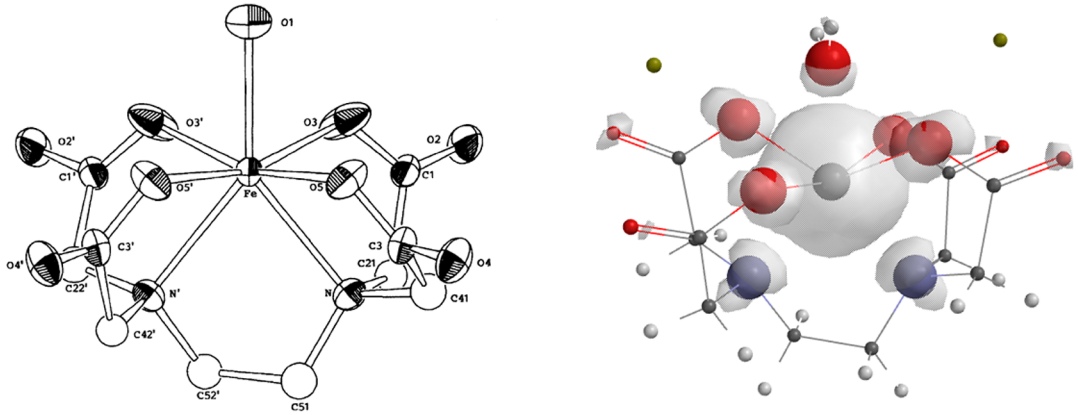

Figure 8. Left side: ORTEP drawing of the Fe(II)(EDTA) dianion (hydrogen atoms omitted for clarity).[31] Right side: B3LYP/6-31G* structure of $K_2Fe(II)(EDTA)(H_2O)$ in the quintet spin state. Fe(II) and ligands coordinating to Fe(II) are displayed as ball and spoke. All other atoms are displayed as ball and wire for clarity. The B3LYP/6-31G* structure in addition shows the spin density (0.002 e/au^3). Reproduced with permission from *Bulletin of the Chemical Society of Japan*.[31] Copyright 1993 The Chemical Society of Japan.

not even $Na_2Fe(II)(EDTA)(H_2O)$ as such but $Na_2[Fe(II)(EDTA)(H_2O)]\cdot 2NaClO_4\cdot 6H_2O$.

An identical approach as for $K_3Fe(II)DTPA$ leads in the case of $K_2Fe(II)q(EDTA)$ to the B3LYP/6-31G* structure shown in Figure 8 on the right side. The two structures show a great resemblance. The Fe−OH_2 distance is 2.267 Å, the four Fe−O (carboxylate) distances are 2.067−2.078 Å, and the two Fe−N distances are 2.272 Å. This structure computationally seems to be a metastable saddle point, as a much more stable structure (ΔE = −172 kJ/mol) was obtained by changing the position of the H_2O molecule. The resulting structure is essentially the same except for the Fe−H_2O distance which now has increased to 3.206 Å while at the same time two hydrogen bridges have formed of 2.084 and 2.114 Å to trans-carboxylate oxygens and the spin density on the H_2O molecule has disappeared. It should be noted that $K_2Fe(II)s(EDTA)$ leads to six-coordination with an octahedral geometry at a much higher in energy.

At this stage no final conclusion can be drawn on the actual structure of Fe(II)q(EDTA) in aqueous solution, as the influence of the two $NaClO_4$ anions and the additional six H_2O molecules in the crystal structure of $Na_2[Fe(II)(EDTA)(H_2O)]\cdot 2NaClO_4\cdot 6H_2O$ has not been dealt with. However, seven-coordination of Fe(II) in a quintet state by four carboxylate oxygens, two nitrogens, and one H_2O molecule in aqueous solution is quite likely.

K_5DTPA. K_5DTPA is the starting material for the dissolution of FeS_2 scale, and therefore its structure in an aqueous environment is important. A similar approach as described for $K_3Fe(II)DTPA$ and $K_2Fe(II)s(EDTA)$ resulted in the structure shown in Figure 9. Again the conformational space seems very limited as the best conformer (MMFF) represents 90% of the Boltzmann distribution. Geometry optimization with B3LYP/6-31G*, including aqueous solvation, does not lead to substantial changes in the structure.

Whereas the very symmetrical front side of the complex is ionic and hydrophilic, the back side of the complex is quite hydrophobic. This might lead to favorable physisorption on the apolar surface of pyrite. This idea is visualized in the graphic in the abstract.

Kinetics. Before an attempt will be made to estimate the overall thermodynamics of the process, the kinetics of the various ligand exchange reactions will be checked. White[29] presented an overview of ligand exchange mechanisms. In Fe(II) (d^6) low spin octahedral complexes dissociative (S_n1) reactions can be expected, while in high spin tetrahedral complexes associative reactions (S_n2) are more likely. Fe(II) ligand exchange reactions are usually quite fast.[25] Figure 10 shows the transition

DOI: 10.1021/acs.iecr.8b01928
Ind. Eng. Chem. Res. 2018, 57, 10095−10104

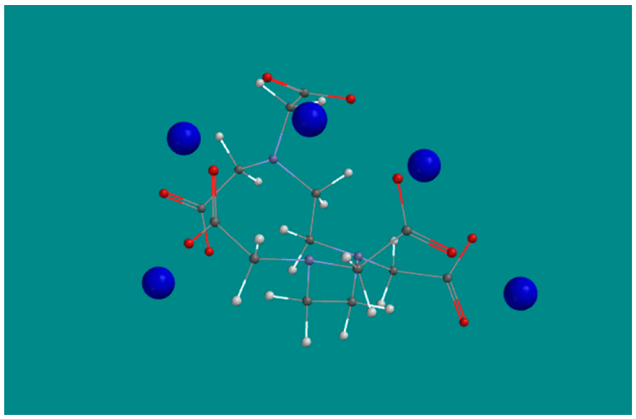

Figure 9. Best conformer (MMFF) of K_5DTPA after geometry optimization with B3LYP/6-31G* with aqueous solvation. The five K^+ ions are displayed as ball and spoke in blue. All other atoms are displayed as ball and wire for clarity reasons.

states of two ligand exchange reactions. The animation of the unique imaginary frequency of TS $Fe(II)q(NH_3)_6(HCO_2)_2$ shows the removal of an NH_3 ligand (Fe−N distance = 3.104 Å) before the formate group comes in. This is a dissociative ligand exchange with an activation barrier of 27.1 kJ/mol.

The animation of the unique imaginary frequency of $K_2Fe(II)(q)(S_2H)_3(OAc)(NH_3)_2$ shows simultaneous movement of the incoming NH_3 ligand and the leaving S_2H ligand. The Fe−N distance of the incoming NH_3 ligand is 2.21 Å, while the Fe−S distance of the leaving S_2H ligand is 3.18 Å. This associative ligand exchange reaction has an activation barrier of 11.4 kJ/mol. Both barriers are almost negligible and in agreement with the literature cited.[29]

Estimate of Thermodynamics. It is not straightforward to set up a computational system for an estimate of the thermodynamics of the descaling reaction. Ideally, the system should look like the equation below:

$$Fe(II)s(S_2)_{solid} + K_5DTPA_{aq} \Leftrightarrow K_3Fe(II)q(DTPA)_{aq} + K_2(S_2)_{aq}$$

However, quantitative DFT results for solids and clusters cannot be taken together as they have different absolute errors, and hence there will be no cancellation of such errors in the calculation of ΔG ($\sim\Delta E$-total energy) of the reaction. This was an important reason to opt for a full cluster approach.

The small cluster $K_4Fe(II)_4s(S_2H)_{12}$ was taken as a model for pyrite. However, $K(S_2H)$ is not a product in aqueous solution but $K_2(S_2)$. This has been accounted for by adding KOH to the equation. Now the equation becomes

$$K_4Fe(II)_4s(S_2H)_{12} + 4K_5DTPA_{aq} + 12KOH_{aq} \Leftrightarrow 4K_3Fe(II)q(DTPA)_{aq} + 12K_2(S_2)_{aq} + 12H_2O_{aq}$$

To this equation, two additional corrections have to be made as these factors largely contribute to the overall ΔE-total energy of the reaction:

(1) The energy of aqueous solvation of KOH, $K_2(S_2)$, and H_2O has to be adapted from $Fe/S_2H = 1/3$ to the molar ratio in bulk pyrite ($Fe/S_2 = 1/1$).
(2) The spin crossover energy calculated for the Fe(II) complexes has to be adapted according the formula derived for $\Delta E_{(HS-LS)}$(CASPT2), listed above.

For a better understanding of the factors contributing to the overall ΔE-total energy of the reaction, the outcome of the gas phase calculations will be presented first:

$$K_4Fe(II)_4s(S_2H)_{12} + 4K_5DTPA + 12KOH \Leftrightarrow 4K_3Fe(II)q(DTPA) + 12K_2(S_2) + 12H_2O$$

The ΔE-total energy of the reaction is −667 kJ/mol $K_4Fe(II)_4s(S_2H)_{12}$ or −167 kJ/mol Fe. Including aqueous solvation of the reaction as such yields −1581 kJ/mol $K_4Fe(II)_4s(S_2H)_{12}$ or −395 kJ/mol Fe. Hence, the contribution of aqueous solvation to the overall ΔE is huge. Removing the aqueous solvation energy of 8 KOH, 8 K_2S_2 and 8 H_2O yields −1032 kJ/mol $K_4Fe(II)_4s(S_2H)_{12}$ or −258 kJ/mol Fe. Finally taking into account the correction of the singlet−quintet spin crossover energy, a ΔE results in −1399 kJ/mol $K_4Fe(II)_4s(S_2H)_{12}$ or −350 kJ/mol Fe. The correction for the singlet−quintet spin crossover energy was calculated from $K_4Fe(II)s(S_2H)_5$ as

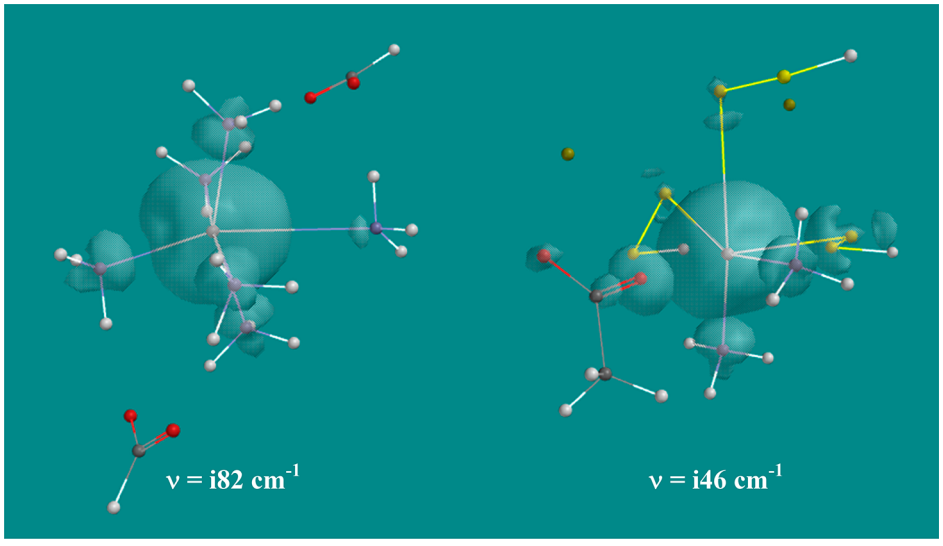

Figure 10. TS $Fe(II)q(NH_3)_6(HCO_2)_2$ and TS $K_2Fe(II)(q)(S_2H)_3(OAc)(NH_3)_2$. B3LYP/6-31G* transition states are displayed as ball and wire. In addition, spin densities (0.002 e/au^3) are displayed.

DOI: 10.1021/acs.iecr.8b01928
Ind. Eng. Chem. Res. 2018, 57, 10095−10104

a model for surface FeS_2 and $K_3Fe(II)q(DTPA)$ as the product.

So the overall ΔE of the computational reaction system chosen is built up from three factors:

(1) a "gas phase" contribution of −167 kJ/mol Fe,
(2) an aqueous solvation contribution of −91 kJ/mol Fe, and
(3) a singlet−quintet spin crossover contribution of −92 kJ/mol Fe.

It should be kept in mind that this estimate is really a rough one, due to the large simplification of the (computational) system, the substantial errors in estimating reaction energies with (standard) DFT insofar as nonisodesmic reactions are involved, and the remaining problem in the correct prediction of the energy differences between high and low spin complexes.

CONCLUSIONS

(1) A plausible sequence of reactions for the stepwise dissolution of pyrite scale by K_5DTPA under basic conditions was developed.

(2) The overall reaction is thermodynamically controlled as only very low activation barriers were calculated, in line with the literature and experimental experiences.

(3) Dissolution of pyrite scale by K_5DTPA under basic conditions is a thermodynamically favorable process. However, the quantitative uncertainty is relatively high due to the number of approximations made and some inherent computational problems.

(4) High spin $K_2Fe(II)(EDTA)(H_2O)$ computationally yields seven-coordination to Fe(II), closely resembling experimental findings. To our knowledge this has not been reported before.

(5) High spin $K_3Fe(II)$DTPA computationally yields seven-coordination to Fe(II), too; however the seven-coordination is built up from three amine ligands and four carboxylate ligands.

ASSOCIATED CONTENT

Supporting Information

The Supporting Information is available free of charge on the ACS Publications website at DOI: 10.1021/acs.iecr.8b01928.

FeS2 scale removal molecular modeling data (XLSX)
PDB structures (ZIP)
Stability test results of high spin complexes (PDF)
Descripton of the content of the other Supporting Information files and a note about restoring properties for PDB files (PDF)

AUTHOR INFORMATION

Corresponding Author

*E-mail: w.buijs@tudelft.nl.

ORCID

Wim Buijs: 0000-0003-3273-5063
Ibnelwaleed A. Hussein: 0000-0002-6672-8649

Notes

The authors declare no competing financial interest.

ACKNOWLEDGMENTS

This publication was made possible by NPRP Grant 9-084-2-041 from Qatar National Research Fund (a member of Qatar Foundation). The findings achieved herein are solely the responsibility of the authors. Qatar University and the Gas Processing Center are acknowledged for their support.

REFERENCES

(1) Olajire, A. A. A review of oilfield scale management technology for oil and gas. production. *J. Pet. Sci. Eng.* **2015**, *135*, 723−737.
(2) Nasr-El-Din, H.; Al-Humaidan, A. Iron Sulfide Scale: Formation, Removal and Prevention. *International Symposium on Oilfield Scale, 30-31 January, Aberdeen, United Kingdom*; Society of Petroleum Engineers, 2001; SPE-68315-MS.
(3) Bader, M. S. H. Sulfate removal technologies for oil fields seawater injection operations. *J. Pet. Sci. Eng.* **2007**, *55* (1−2), 93−110.
(4) Crabtree, M.; Eslinger, D.; Fletcher, P.; Miller, M.; Johnson, A.; King, G. Fighting scale: removal and prevention. *Oilfield Rev.* **1999**, *11* (3), 30−45.
(5) Yap, J.; Fuller, M. J.; Schafer, L.; Kelkar, S. K. Removing Iron Sulfide Scale: A Novel Approach. Presented at Abu Dhabi International Petroleum Exhibition and Conference, Society of Petroleum Engineers, 2010.
(6) Rickard, D.; Luther, G. W., III. Chemistry of iron sulfides. *Chem. Rev.* **2007**, *107*, 514−562.
(7) Li, J.; Li, T.; Yan, J.; Zuo, X.; Zheng, Y.; Yang, F. How Scaling Impacts Sucker Rod Pump. Presented at Asia Pacific Oil and Gas Conference & Exhibition, Society of Petroleum Engineers, 2009.
(8) Senthilmurugan, B.; Ghosh, B.; Sanker, S. J. High performance. maleic acid based on oil well scale inhibitors-development and. comparative evaluation. *J. Ind. Eng. Chem.* **2011**, *17* (3), 415−420.
(9) Chilingar, G. V.; Mourhatch, R.; Al-Qahtani, G. *the Fundamentals of Corrosion and Scaling for Petroleum and Environmental Engineers*; Gulf Publishing Company, 2008.
(10) Corrosion in the Oil and Gas Industry. https://www.nace.org/Corrosion-Central/Industries/Oil---Gas-Production (accessed Feb 22, 2018).
(11) Sulaiman, K. O.; Onawole, A. T. Quantum chemical evaluation of the corrosion inhibition of novel aromatic hydrazide derivatives on mild steel in hydrochloric acid. *Comput. Theor. Chem.* **2016**, *1093*, 73−80.
(12) Kabir, A. H.; Haron, J. Scaling Challenges in Tinggi Operation. Presented at International Symposium on Oilfield Scale, Society of Petroleum Engineers, 2000.
(13) Chen, T.; Wang, Q.; Chang, F. F.; Al-Janabi, Y. T. Removing a Typical Iron Sulfide Scale: The Scientific Approach. *SPE Rocky Mountain Regional Meeting, 18-21 May, Casper, Wyoming*; Society of Petroleum Engineers, 2016; DOI: 10.2118/24327.
(14) Wang, X.; Qu, Q.; Berry, S.; Cutler, J. Iron Sulfide Removal: A Nonacidic Alternative to Hydrochloric Acid Treatment. Presented at the 10th SPE International Conference and Exhibition on European Formation Damage, Noordwijk, The Netherlands, Jun 5−7, 2013; SPE 165199-MS.
(15) Fleming, N. Investigation of the use of scale risk parameters to predict failure of downhole safety valves on the Gullfaks Field. Presented at Gullfaks-Scaling Risk Evaluation Challenges, SPE Scale Workshop, Abu Dhabi, 2010.
(16) Mahmoud, M.; Hussein, I. A.; Sultan, A.; Saad, M. A.; Buijs, W.; Vlugt, T. J. H. Development of Efficient Formulation for the Removal of Iron Sulfide Scale in Sour Production Wells. accepted for publication in. *Can. J. Chem. Eng.* **2018**, DOI: 10.1002/cjce.23241.
(17) Grønvold, F.; Westrum, E. F. Heat capacities of iron disulfides Thermodynamics of marcasite from 5 to 700 K, pyrite from 300 to 780 K, and the transformation of marcasite to pyrite. *J. Chem. Thermodyn.* **1976**, *8* (11), 1039−1048.
(18) Wang, K.-S.; Resch, R.; Dunn, K.; Shuler, P.; Tang, Y.; Koel, B. E.; Fu Yen, T. Interactions between Mineral Surfaces and Dissolved Species: From Monovalent Ions to Complex Organic Molecules. *Colloids Surf., A* **1999**, *160* (3), 217−227.
(19) Martell, A. E.; Motekaitis, R. J.; Chen, D.; Hancock, R. D.; McManus, D. Selection of new Fe(lll)/Fe(ll) chelating agents as catalysts for the oxidation of hydrogen sulfide to sulfur by air. *Can. J. Chem.* **1996**, *74*, 1872−1879.
(20) Moghadasi, J.; Müller-Steinhagen, H.; Jamialahmadi, M.; Sharif, A. Model. study on the kinetics of oil field formation damage due to

salt precipitation. from injection. *J. Pet. Sci. Eng.* **2004**, *43* (3−4), 201−217.
(21) Haghtalab, A.; Kamali, M. J.; Shahrabadi, A.; Golghanddashti, H. Investigation of the Precipitation of Calcium Sulfate in Porous Media: Experimental and Mathematical Modeling. *Chem. Eng. Commun.* **2015**, *202* (9), 1221−1230.
(22) Tomasi, J.; Mennucci, B.; Cammi, R. Quantum mechanical continuum solvation models. *Chem. Rev.* **2005**, *105*, 2999−3093.
(23) Wavefunction Inc., Irvine, CA. www.wavefun.com (accessed 2017).
(24) Bowman, D. N.; Jakubikova, E. Low-Spin versus High-Spin Ground State in Pseudo-Octahedral Iron Complexes. *Inorg. Chem.* **2012**, *51* (11), 6011−6019.
(25) Draksharapu, A.; Li, Q.; Logtenberg, H.; van den Berg, T. A.; Meetsma, A.; Killeen, J. S.; Feringa, B. L.; Hage, R.; Roelfes, G.; Browne, W. R. Ligand Exchange and Spin State Equilibria of Fe-II(N4Py) and Related Complexes in Aqueous Media. *Inorg. Chem.* **2012**, *51* (2), 900−913.
(26) Franke, P. L.; Haasnoot, J. G.; Zuur, A. P. Tetrazoles as ligands. Part IV. lron(ll) complexes of monofunctional tetrazole ligands, showing high-spin (5T29) low-spin transitions. *Inorg. Chim. Acta* **1982**, *59*, 5−9.
(27) Swart, M. Accurate Spin-State Energies for Iron Complexes. *J. Chem. Theory Comput.* **2008**, *4* (12), 2057−2066.
(28) Lawson Daku, L. M.; Vargas, A.; Hauser, A.; Fouqueau, A.; Casida, M. E. Assessment of density functionals for the high-spin/low-spin energy difference in the low-spin iron(II) tris(2,2′-bipyridine) complex. *ChemPhysChem* **2005**, *6* (7), 1393−1410.
(29) White, M. C. Ligand Exchange Mechanisms. *Chem* **2002**, *153*, 43−53.
(30) Grau, M.; England, J.; Torres Martin De Rosales, R.; Rzepa, H. S.; White, A. J. P.; Britovsek, G. J. P. Coordination Equilibria Between Seven- and Five-coordinate Iron(II) Complexes. *Inorg. Chem.* **2013**, *52* (20), 11867−11874.
(31) Mizuta, T.; Wang, J.; Miyoshi, K. A Seven-Coordinate Structure of Iron(II)−Ethylenediamine-N,N,N′,N′-tetraacetato Complex as Determined by X-Ray Crystal Analysis. *Bull. Chem. Soc. Jpn.* **1993**, *66*, 2547−2551.
(32) Pierloot, K.; Vancoillie, S. Relative energy of the high-($^5T_{2g}$) and low-($^1A_{1g}$) spin states of the ferrous complexes [Fe(L)(NHS_4)]: CASPT2 versus density functional theory. *J. Chem. Phys.* **2008**, *128*, 034104.
(33) Chemistry. LibreTexts. https://chem.libretexts.org/Core/Inorganic_Chemistry/Crystal_Field_Theory/High_Spin_and_Low_Spin_Complexes.
(34) Nickel, H. E. Structural Stability of Minerals with Pyrite, Marcasite, Arsenopyrite and Löllingite Structures. *Can. Mineral.* **1968**, *9* (3), 311−321.
(35) American Mineralogist Structure Database. http://rruff.geo.arizona.edu/AMS/amcsd.php.
(36) Buhks, E.; Navon, G.; Bixon, M.; Jortner, J. Spin conversion processes in solutions. *J. Am. Chem. Soc.* **1980**, *102*, 2918−2923.
(37) Mandado, M.; Cordeiro, M. N. D. S. On the Stability of Metal−Aminoacid Complexes in Water Based on Water−Ligand Exchange Reactions and Electronic Properties: Detailed Study on Iron−Glycine Hexacoordinated Complexes. *J. Comput. Chem.* **2010**, *31*, 2735−2745.
(38) https://chem.libretexts.org/Textbook_Maps/Physical_and_Theoretical_Chemistry_Textbook_Maps/Supplemental_Modules_(Physical_and_Theoretical_Chemistry)/Electronic_Structure_of_Atoms_and_Molecules/Electronic_Configurations/Spin_Pairing_Energy.
(39) Seeger, R.; Pople, J. A. Self-consistent molecular orbital methods. XVIII. Constraints and stability in Hartree−Fock theory. *J. Chem. Phys.* **1977**, *66*, 3045.

DOI: 10.1021/acs.iecr.8b01928
Ind. Eng. Chem. Res. 2018, 57, 10095−10104